Talanta 120 (2014) 484–490

Contents lists available at ScienceDirect

Talanta

journal homepage: www.elsevier.com/locate/talanta

Highly sensitive nonenzymatic glucose and H_2O_2 sensor based on $Ni(OH)_2$/electroreduced graphene oxide – Multiwalled carbon nanotube film modified glass carbon electrode

Wei Gao [a], Weng Weei Tjiu [b], Junchao Wei [a], Tianxi Liu [a,*]

[a] State Key Laboratory of Molecular Engineering of Polymers, Department of Macromolecular Science, Fudan University, Shanghai 200433, China
[b] Institute of Materials Research and Engineering, A*STAR (Agency for Science, Technology and Research), 3 Research Link, Singapore 117602, Singapore

ARTICLE INFO

Article history:
Received 5 September 2013
Received in revised form
3 December 2013
Accepted 5 December 2013
Available online 27 December 2013

Keywords:
Graphene
Multiwalled carbon nanotubes
$Ni(OH)_2$
Glucose sensor
Hydrogen peroxide sensor

ABSTRACT

In this article, a nonenzymatic sensor based on $Ni(OH)_2$/electroreduced graphene oxide (ERGO)–multiwalled carbon nanotube (MWNT) nanocomposites is fabricated via convenient electrodeposition of $Ni(OH)_2$ nanoparticles on ERGO–MWNT film modified glass carbon electrode (GCE). Graphene oxide (GO) sheets can serve as surfactants to stabilize the dispersion of pristine MWNTs in aqueous solution, rendering a fine coverage of ERGO–MWNT film on GCE during the fabrication process. MWNTs perform as conducting bridges between ERGO sheets to enhance the electron transfer rate in the substrate. By combining the advantages of ERGO and MWNTs, together with electrocatalytic effect of $Ni(OH)_2$ nanoparticles, the well-designed nanocomposites exhibit excellent sensing behavior towards glucose and hydrogen peroxide (H_2O_2). The linear detection ranges for glucose and H_2O_2 are 10–1500 μM and 10 μM–9050 μM while the detection limits are 2.7 μM and 4.0 μM, respectively. Furthermore, a very high sensitivity is achieved with 2042 μAm M^{-1} cm^{-2} estimated for glucose and 711 μAm M^{-1} cm^{-2} for H_2O_2. These results suggest that $Ni(OH)_2$/ERGO–MWNT nanocomposites thus easily prepared through a green electrochemical method are promising electrode materials for biosensing. Additionally, good recoveries of analytes in real samples like urine and milk confirm the reliability of the prepared sensor in practical applications.

1. Introduction

Nanocarbon materials are coming to the forefront of the electrochemical biosensing field because of their extraordinary physical properties and remarkable conductivity [1]. The one-dimensional (1D) carbon nanotubes have achieved great attentions in determination of various analytes as electrode modifiers [2–4], due to their excellent electron transferability, high aspect ratio and chemical stability [5]. Graphene, a well-defined two-dimensional (2D) lattice structure of carbon atoms possessing excellent physicochemical properties, is also regarded as an outstanding catalyst support for nonenzymatic biosensing [6,7]. Graphene oxide (GO), the oxidation form of graphene, obtained by treating graphite with strong oxidizer, containing multiple aromatic regions and hydrophilic oxygen groups, can facilitate the suspension of undispersible pristine multiwalled carbon nanotubes (MWNTs) in aqueous solution by forming GO–MWNT complexes through strong π–π stacking interaction [8–10]. The suspension of GO–MWNT complexes is well processible for the fabrication of electrode architectures [11]. Furthermore, despite of dissimilarity in structure, the reduced GO (rGO) shows similar properties with MWNTs, and the noncovalent rGO–MWNT complexes thus formed presumably have synergistic effects and can act as building blocks for developing novel carbon nanomaterials with potentially improved conductivity and catalytic effect for electrochemical research [12]. Wang et al. have reported a hydrogen peroxide (H_2O_2) sensor of PtAu bimetallic nanoparticles synthesized on graphene–MWNT complexes via the one-step co-reduction method [13]. Chu et al. have reported rGO/single-walled carbon nanotubes (SWNT) nanocomposites as modifier on glass carbon electrode (GCE) used for biochemical sensing towards H_2O_2 and β-nicotinamide adenine dinucleotide (NADH) [14].

Diabetes, a common chronic disease, is becoming a great threat to the health of humanity now. Many reliable and efficient methods have been developed to monitor glucose in human blood for clinical detection and therapy. Although good selectivity and high sensitivity can be obtained with those glucose sensors immobilized with enzymes, the drawbacks originated from the intrinsic features of enzyme such as thermal or chemical instabilities greatly hinder their practical applications [15]. Thus,

* Corresponding author. Tel.: +86 21 55664197; fax: +86 21 65640293.
E-mail address: txliu@fudan.edu.cn (T. Liu).

0039-9140/$ - see front matter © 2013 Elsevier B.V. All rights reserved.
http://dx.doi.org/10.1016/j.talanta.2013.12.012

nonenzymatic sensors based on metals and their derivatives such as Cu [16], $Ni(OH)_2$ [17] and MnO_2 [18] are broadly investigated to overcome these disadvantages. H_2O_2, the product of glucose oxidation in the presence of glucose oxidase and oxygen [19], as well as an essential compound widely used in food, clinical, environment and pharmaceutical fields, also draws increasing attentions for its quantitative detection [20]. A diversity of H_2O_2 sensors, like those based on noble metals such as Ag [21], Au [22], has been reported to possess good electrocatalytic activities.

Among all those relatively low cost materials, Ni based nanocomposites display high electrochemical properties as sensors for glucose [23], H_2O_2 [24] and ethanol [25]. During the detection, oxydroxide species (NiOOH) tend to be formed in alkaline media and further catalyze the oxidation process of the analytes [26]. Decorating these Ni derivatives as isolated nanoparticles or nanostructures with different morphologies on the substrate offers a popular strategy to develop efficient electrocatalytic sensors. The synergistic effect of metal catalysts and the substrate they were grown on may result in enhanced detection properties.

In this report, we have proposed a new and convenient strategy to fabricate ternary $Ni(OH)_2$/electroreduced graphene oxide (ERGO)–MWNT nanocomposites for glucose and H_2O_2 detection. ERGO–MWNT hybrid film was modified on GCE by dropping the suspension of well dispersible GO–MWNT complexes on the electrode surface. In the following steps, the electroreduction was performed as a green and fast method to convert GO to ERGO without any contamination of the reduced material [27], with high aspect ratio pristine MWNTs promoting this process [28]. $Ni(OH)_2$ nanoparticles were grown on ERGO–MWNT substrates by a simple electrodeposition method. The synergistic effect of ERGO and MWNTs makes the hybrid film a unique electrocatalytic support for the growth or formation of $Ni(OH)_2$ nanoparticles. The sensor thus prepared demonstrates a notable nonenzymatic sensing behavior towards glucose and H_2O_2, with high sensitivity, large linear range, short response time and low detection limit.

2. Experimental

2.1. Reagents and materials

Natural graphite powder (325 mesh) was purchased from Alfa Aesar. MWNTs (length, 10–30 μm; outer diameter, 20–30 nm; purity, 95%) were supplied by Chengdu Institute of Organic Chemistry. 98% H_2SO_4, KNO_3, $KMnO_4$, $NaNO_3$, NaCl, NaOH, HCl, N,N-dimethylformamide (DMF), glucose, fructose, galactose and ascorbic acid (AA) were obtained from Sinopharm Chemical Reagent Co. Ltd. Uric acid (UA, 98%) was received from J&K Scientific Co. Ltd. $NiCl_2 \cdot 6H_2O$ was commercially received from Aldrich. Phosphate buffer solutions (PBS, pH=7, 0.2 M) were prepared by blending standard solutions of Na_2HPO_4 and NaH_2PO_4. Dilute solutions of H_2O_2 were freshly prepared daily. Deionized (DI) water was used throughout the experiments.

2.2. Preparation of $Ni(OH)_2$/ERGO–MWNT/GCE

The strategy of the whole experiment is presented in Scheme 1. Graphite oxide was prepared according to modified Hummer's method. The obtained products were exfoliated in DI water by ultrasonicating for 1 h. Then GO suspension was used to disperse pristine MWNTs by pouring them onto MWNT conglomerations with another ultrasonication for 1 h. Suspensions of GO–MWNT complexes with different GO/MWNT weight ratios (1/1, 2/1,and 4/1) were prepared and directly used to modify the electrodes. All suspensions were kept at a constant concentration of 2 mg/mL. Before being used, bare GCE (diameter: 3 mm) was polished with

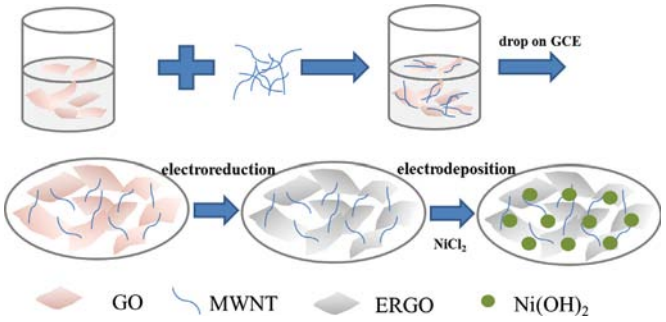

Scheme 1. Schematic illustration of the fabrication of $Ni(OH)_2$/ERGO–MWNT/GCE.

1.0, 0.3 and 0.05 μm alumina slurry, and then ultrasonicated in a 1:1 ethanol/water solution for 15 min to remove the residual alumina, and finally dried in the nitrogen flow. GO–MWNT film was coated on GCE by dropping 5 μL of GO–MWNT suspension on the electrode surface, followed by drying in a desiccator over silica gel. Then, the reduction of GO–MWNT/GCE was performed on the electrochemical station in 0.2 M PBS solution at a cyclic-voltage potential range of 0– – 1.5 V with a scan rate of 100 m V s^{-1}. Then the electrodeposition of $Ni(OH)_2$ nanoparticles was carried out at ERGO–MWNT/GCE in the presence of 10 mM Ni^{2+} under a constant potential of − 1.1 V for 15 s [29].

For comparison, $Ni(OH)_2$/ERGO/GCE and $Ni(OH)_2$/MWNT/GCE were also fabricated through the same procedure except that pure GO suspension or pristine MWNTs dispersed in DMF were used as modifiers on GCE for $Ni(OH)_2$ electrodeposition. $Ni(OH)_2$/GCE was fabricated by directly electrodepositing $Ni(OH)_2$ on bare GCE.

2.3. Measurements and apparatus

All electrochemical measurements were performed on a CHI 660D electrochemical workstation. A three-electrode system was used throughout the experiments with a modified GCE as working electrode, a platinum wire as auxiliary electrode, and an Ag/AgCl (3 M KCl) electrode as reference electrode. All these electrochemical measurements were performed under ambient temperature. Raman spectra were conducted on a JobinYvon LABRAM-1B Raman spectrometer at an exciting wavelength of 632.8 nm. Transmission electron microscopy (TEM) images were acquired under an acceleration voltage of 200 kV with a Philips CM 300 FEG TEM. Scanning electron microscopy (SEM) was performed with a JEOL JSM-7600F coupled with an energy-dispersive X-ray (EDX) detector. Before SEM observations, the sample surfaces were coated with gold.

3. Results and discussion

3.1. Characterization of GO–MWNT complexes

Fig. 1a clearly shows that pristine MWNT conglomerations just aggregate in aqueous solution and precipitate to the bottom of the vessel. In contrast, GO, due to the hydrophilic groups attached on the plane, can be well dispersed and form a brown yellow colloidal suspension. However, when the pristine MWNTs were mixed with GO at a weight ratio of 1/4 and after sonication, the pristine MWNTs can be successfully suspended by GO sheets and form a uniform black suspension. TEM micrograph in Fig. 1b shows that the surfaces of GO sheets are bestrewed with the MWNTs, indicating the formation of GO-MWNT complexes due to the strong π–π stacking interaction between GO and MWNTs. And the content of MWNTs does not lead to serious aggregation of the complex.

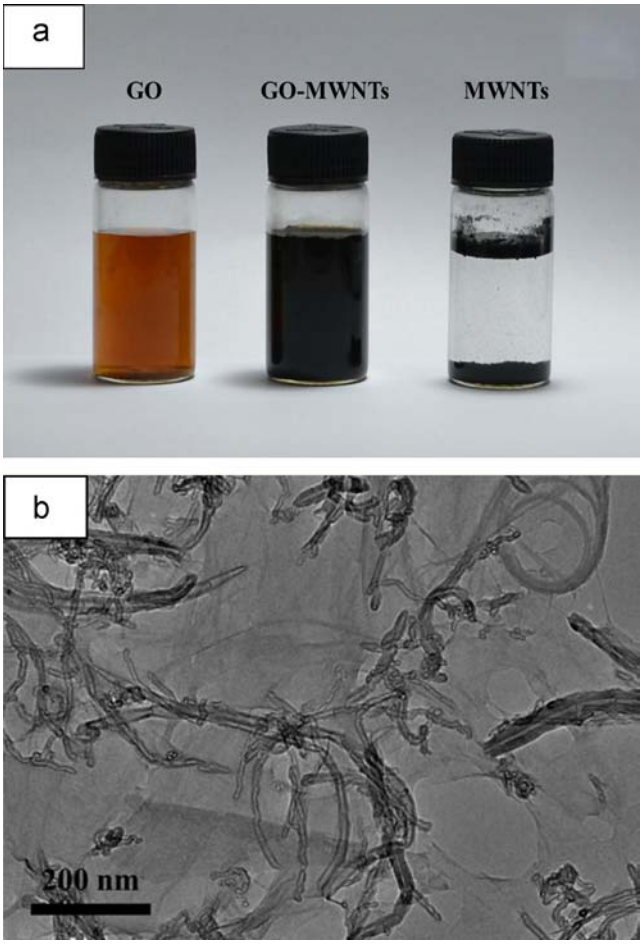

Fig. 1. (a) Photograph of GO, GO–MWNT (4:1) complexes and pristine MWNTs dispersed in aqueous solution. (b) TEM image of GO–MWNT complex.

Raman spectra of MWNTs, GO and GO–MWNT complexes are presented in Fig. 2. All the Raman spectra exhibit two bands, G band and D band. The D band is related to the presence of sp^3 defects while the G band is related to the in-plane vibration of sp^2 carbon atoms [30]. It can be seen that the relative intensity ratio (I_G/I_D) of the GO–MWNT complexes is higher than that of pure GO, indicating that the introduction of pristine MWNTs into the complexes has lowered the relative content of sp^3 defects, which is conducive to the electron transfer.

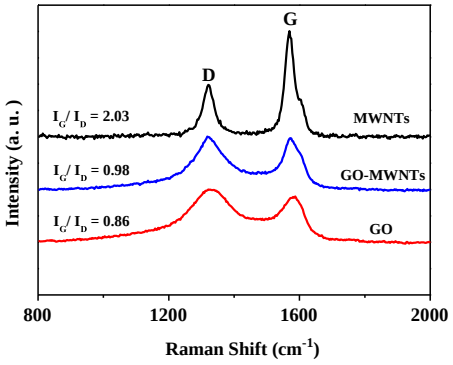

Fig. 2. Raman spectra of pristine MWNTs, GO and GO–MWNT complexes.

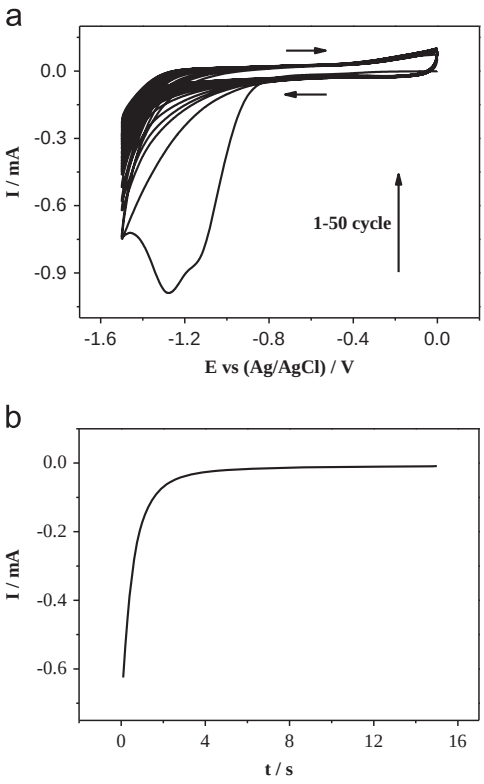

Fig. 3. (a) CVs of GO–MWNT/GCE in 0.2 M PBS aqueous solution (pH=7) at a scan rate of 100 mV s^{-1}. The horizontal arrows indicate the scan direction. (b) Current (I)–time (t) curve of ERGO–MWNT/GCE under constant potential of −1.1 V for 15 s in 10 mM $NiCl_2 \cdot 6H_2O$ solution.

3.2. *Electrosynthesis of $Ni(OH)_2$/ERGO–MWNT/GCE*

When the suspension of GO–MWNT complexes was dropped on the surface of the electrode and vacuum dried, a uniform film was formed on GCE. Fig. 3a shows the cyclic voltammograms (CVs) of the GO–MWNT film modified GCE in a potential range from 0 to −1.5 V for 50 cycles. In the first cycle, a strong cathodic current peak at −1.27 V with a starting potential from −0.83 V is observed, due to the reduction of the oxygen groups attached to the GO surface since the reduction of water to hydrogen occurs at a more negative potential (e.g., −1.5 V). In the following cycles, the reduction peak decreases and finally disappears while the curve tends to stabilize, indicating that the electroreduction of GO occurs irreversibly and the oxygenated species are eliminated [27]. In this way, GO–MWNT film modified on GCE is changed or reduced to ERGO–MWNT film with better stability and enhanced electron transferability. The current (I)–time (t) curve of $Ni(OH)_2$ electrodeposition process is presented in Fig. 3b. In the latter seconds, a constant current is met, corresponding to a constant flux of [OH^-] at the electrode surface [17].

3.3. *Structure and morphology of $Ni(OH)_2$/ERGO–MWNT nanocomposites*

Surface morphologies of the electrode modifiers are further investigated. Fig. 4(a,b) shows the SEM images of GO–MWNT hybrid film formed on the ITO glass. Close inspection indicates that the film surface displays characteristic features of the wrinkles of GO sheets, coexisting with the typical tube-like MWNT features. Here, GO plays the roles of dispersing agent, smoothing the surface and retarding or inhibiting the aggregation of the MWNTs [14]. MWNTs intersperse randomly among the GO sheets and interwine with each other to form a homogenous three-dimensional (3D) network. The insertion of MWNTs or the adsorption of MWNTs on the GO

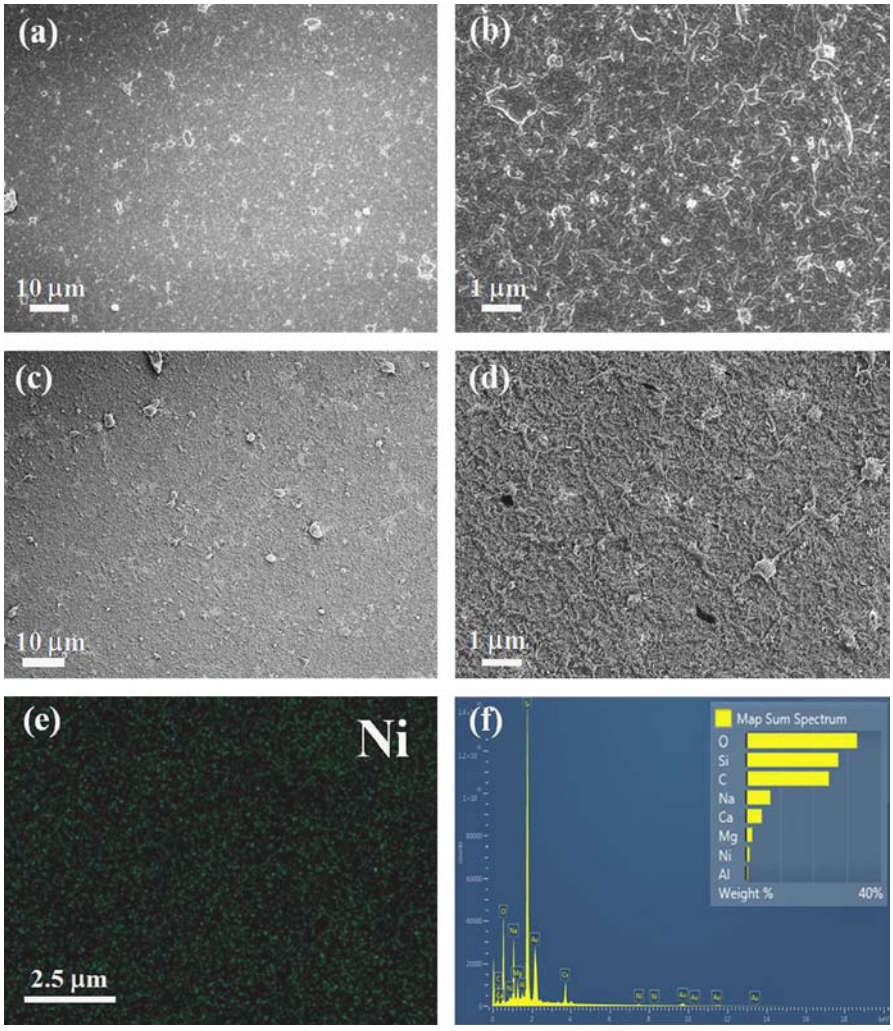

Fig. 4. SEM images at low (left) and high (right) magnifications for GO–MWNT film (a, b) and $Ni(OH)_2$/ERGO–MWNT nanocomposites (c, d) deposited on ITO. (e) The elemental mapping for Ni in $Ni(OH)_2$/ERGO–MWNT modified ITO. (f) The corresponding EDX spectrum taken from the whole area.

surface via π–π interaction (see Fig. 1b) greatly prevents the GO sheets themselves from restacking, resulting in a larger surface area. However, for the $Ni(OH)_2$/ERGO–MWNT nanocomposite film modified on ITO, Fig. 4(c,d) demonstrate that a rougher surface is obtained after electroreduction process in PBS and the subsequent electrodeposition of $Ni(OH)_2$ nanoparticles, while the features of ERGO–MWNT substrate are still evident. EDX results (Fig. 4e, f) prove that the deposited $Ni(OH)_2$ nanoparticles have an even distribution on the carbonaceous substrate with very small sizes, and no obvious aggregation is found.

3.4. Optimization of the experimental results

In order to optimize the electrochemical property, $Ni(OH)_2$ nanoparticles were electrodeposited on ERGO–MWNT substrate with different initial GO/MWNT weight ratios (4/1, 2/1, and 1/1) by the same procedures and their electrochemical behaviors in alkaline medium were investigated. The CVs shown in Fig. S1 indicate that the nanocomposite based on complex with GO/MWNT weight ratio of 4/1 is found to exhibit the strongest redox peaks in 0.1 M NaOH solution with an increased background current, compared with $Ni(OH)_2$ deposited on pure ERGO alone, implying that it possesses the best electrochemical property in electrode modification. With this weight ratio, MWNTs may be able to enhance the impeded charge transferability among the isolated ERGO sheets by constructing conductive bridges, leading to improved electrochemical properties as well as larger electroactive surface area of the 3D complexes. However, further increasing the contents of MWNTs in the complex may lead to the aggregation and an uneven surface of the hybrid film which will hinder the deposition of $Ni(OH)_2$ nanoparticles, and thus the performance of $Ni(OH)_2$/ERGO–MWNT nanocomposites may be affected. Considering the above, the GO/MWNT ratio of 4/1 is considered as the optimum proportion in the complex for the substrate and used in the following experiments.

3.5. Electrochemical sensing of glucose using $Ni(OH)_2$/ERGO–MWNT/GCE

3.5.1. Electrocatalytic effect towards glucose

With the combination of good electrochemical property of ERGO–MWNT support and the catalytic activity of $Ni(OH)_2$ nanoparticles, the sensing behavior of the prepared electrodes towards glucose oxidation is investigated by employing CVs within a potential range from 0.2 V to 0.6 V at a scan rate of 100 mV/s. Fig. 5a shows the CVs of ERGO–MWNT/GCE, $Ni(OH)_2$/GCE, $Ni(OH)_2$/MWNT/GCE, $Ni(OH)_2$/ERGO/GCE and $Ni(OH)_2$/ERGO–MWNT/GCE in 0.1 M NaOH containing 2 mM glucose. No redox peaks are observed for ERGO–MWNT/GCE and a pair of small peaks are observed for $Ni(OH)_2$/GCE, which are assigned to the oxidation and reduction of Ni species in the presence of glucose.

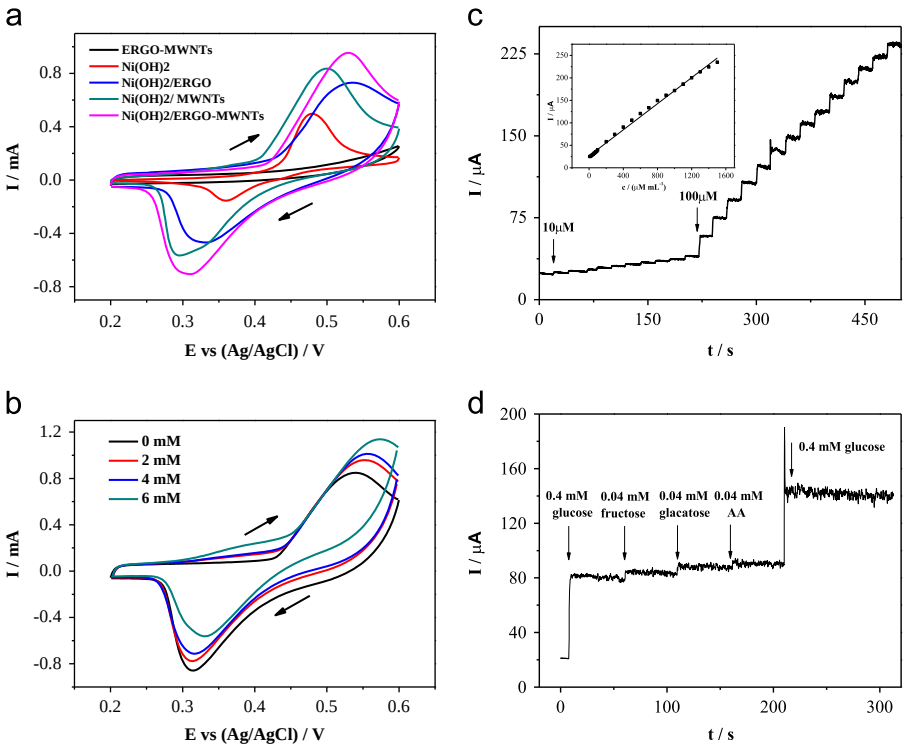

Fig. 5. (a) CVs of $Ni(OH)_2$, ERGO–MWNT, $Ni(OH)_2$/ERGO, $Ni(OH)_2$/MWNT, $Ni(OH)_2$/ERGO–MWNT modified GCE in the presence of 2 mM glucose at a scan rate of 100 mV s^{-1}. (b) CVs of $Ni(OH)_2$/ERGO–MWNT/GCE with different concentrations of glucose. The arrows indicate the scan direction. (c) Typical amperometric response of $Ni(OH)_2$/ERGO–MWNT/GCE to successive addition of glucose, applied potential was 0.54 V. Inset: the corresponding calibration curve of *I*–*C* obtained by chronoamperometry. (d) Interference test at $Ni(OH)_2$/ERGO–MWNT/GCE at 0.54 V. The supporting electrolyte is 0.1 M NaOH.

However, when $Ni(OH)_2$ nanoparticles are deposited on carbonaceous modifiers rather than on bare GCE, the anodic/cathodic current response obviously increases and a couple of well-defined redox peaks appear. However, the sensor based on ERGO–MWNT film modified GCE yields a higher enhancement and stronger peak currents than those based on ERGO or MWNTs individually. Since the oxidation reaction takes place at the interfaces between $Ni(OH)_2$ nanoparticles and analytes, the synergistic effect between 2D ERGO and 1D MWNTs makes the 3D hybrid substrate a better platform for electron transfer between $Ni(OH)_2$ nanoparticles and GCE.

The most electroactive sensor of $Ni(OH)_2$/ERGO–MWNT/GCE was investigated for glucose detection. The dependence of the CVs on the glucose concentration is presented in Fig. 5b.With the increase of the glucose concentration in the electrolyte, the anodic peak current increases and shifts to a more positive value while the cathodic peak shifts towards the same direction. This phenomenon is due to NiOOH/$Ni(OH)_2$ redox couple electrocatalyzed oxidation process of glucose to gluctone, as shown in the following reactions [23]:

$$Ni(OH)_2 + OH^- \leftrightarrow NiOOH + H_2O + e^- \quad (1)$$

$$NiOOH + \text{glucose} \rightarrow Ni(OH)_2 + \text{glucolactone} \quad (2)$$

3.5.2. *Chronoamperometric response to glucose and calibration curve*

Fig. 5c illustrates the typical current(*I*)–time(*t*) curve of $Ni(OH)_2$/ERGO–MWNT/GCE to successive glucose addition with an applied potential set at 0.54 V, and the amplification of the marked rectangle region is presented in lower right inset. When a certain amounts of glucose (10 μM, 100 μM) were injected into the stirring solution of 0.1 M NaOH, the current got a sharp increase and then achieved a steady state within a rapid response time of 2.0 s. The calibration curve is presented in the upper left inset, showing a good linear relationship (coefficient $R^2 = 0.996$) between current and glucose concentration (*C*) from 10 μM to 1500 μM. The corresponding linear regression equation is written as $I(\mu A) = 26.453 + 0.145C\,(\mu M)$. From the equation, the detection limit and the sensitivity are calculated to be 2.7 μM (signal-to-noise ratio = 3) and 2042 μA mM^{-1} cm^{-2}, respectively. The $Ni(OH)_2$/ERGO–MWNT nanocomposites we prepared exhibit a comparable sensing performance to those nonzymatic sensors reported previously, especially showing a high sensitivity, as listed in Table 1. Moreover, the simple and green eletrochemical method used here is the main advantage for fabricating this new kind of sensor.

Table 1
Comparison of the performances of different glucose sensors.

Sensor	Detection limit (μM)	Linear range (mM)	Sensitivity (μA mM^{-1} cm^{-2})	Reference
RGO–$Ni(OH)_2$/GCE	0.6	0.002–3.1	11.43	[23]
NiCFP[a]	1	0.002–2.5	420.4	[32]
NiO–MWCNTs	160	0.2–1.2	Not given	[33]
GO/NiO nanofibers	0.77	0.002–0.6	1100	[34]
Ni-BBD[b]	2.7	0.01–10	1040	[35]
Ni nanosphere-RGO	1	0.001–0.11	813	[36]
$Ni(OH)_2$/ERGO–MWNT/GCE	2.7	0.01–1.5	2042	This work

[a] Ni loaded carbon nanofiber paste electrode.
[b] Ni-BBD:Ni modified boron-doped diamond electrode.

3.5.3. Selectivity, reproducibility and stability for glucose detection

In the interference study, a number of interfering species such as fructose, glacatose andascrobic acid (AA) were sequentially added and examined by $Ni(OH)_2$/ERGO–MWNT/GCE during the glucose detection (Fig. 5d). Strong glucose responses are observed along with weak responses of the interfering species. Considering their relative concentrations in the real sample such as human blood, the modified electrode reveals an acceptable selectivity towards glucose detection. Reproducibility was tested by independently measuring CVs of six modified electrodes in 0.1 M NaOH containing 2 mM glucose, and a relative standard deviation (RSD) of 2.8% is estimated for the oxidation peak currents. The stability of the sensor was also studied by recording the amperometric response of the electeode for 100 μM glucose. No obvious current decline observed in the current–time curve after six successive measurements, and the RSD is calculated to be 5.9%. Therefore, this kind of nonenzymatic glucose sensor displays good reproducibility and stability.

3.6. Electrochemical sensing of H_2O_2 using $Ni(OH)_2$ /ERGO–MWNT/GCE

3.6.1. Electrocatalytic effect towards H_2O_2

CVs were employed to investigate the electrocatalytic performance of sensors towards H_2O_2. As shown in Fig. 6a, $Ni(OH)_2$ containing electrodes demonstrate higher background current compared with ERGO–MWNT/GCE due to the oxidation and reduction reactions, and the sensor based on $Ni(OH)_2$/ERGO–MWNT/GCE exhibits the maximum signals in the presence of 10 mM H_2O_2 in terms of anodic and cathodic peak currents, indicating that it has the most favorable catalytic ability towards H_2O_2, better than the electrodes made of $Ni(OH)_2$ deposited on ERGO, MWNT substrate or non-substrate. The CVs obtained in the presence of different concentrations of H_2O_2 are presented in Fig. 6b. By increasing H_2O_2 concentration, a notable enhancement of current response in the positive scan is achieved accordingly, as the reduction of NiOOH and the oxidation of H_2O_2 occur simultaneously. The electrochemical pathway responsible for the catalytic effect of ERGO–MWNT/$Ni(OH)_2$ towards H_2O_2 can be described as follows [31]:

$$Ni(OH)_2 + OH^- \leftrightarrow NiOOH + H_2O + e^- \quad (3)$$

$$2NiOOH + H_2O_2 \rightarrow 2Ni(OH)_2 + O_2\uparrow \quad (4)$$

3.6.2. Chronoamperometric response to H_2O_2 and calibration curve

To further confirm the electrocatalytic activity of $Ni(OH)_2$/ERGO–MWNT/GCE, the chronoamperometric response towards successive injection of certain amounts of H_2O_2 (e.g., 10 μM, 100 μM and 500 μM) at the set potential of 0.2 V is presented in Fig. 6c. It can be seen that the electrode responds quickly to the added analytes in a short response time of 2 s. The calibration plot of the current as a function of H_2O_2 concentration is shown in the upper inset, revealing a good linearity (coefficient $R^2 = 0.997$) within the range from 10 μM to 9050 μM. The corresponding linear regression equation is: I (μA) = 11.531 + 0.051C (μM). The detection limit is thus estimated to be 4.0 μM (signal-to-noise ratio = 3) and the sensitivity is obtained to be 717 μA mM^{-1} cm^{-2}. These results are also compared with other biosensors used for H_2O_2 electroanalysis, as listed in Table 2. Clearly, the $Ni(OH)_2$/ERGO–MWNT electrode shows comparable and even better analytical performance.

3.6.3. Selectivity, reproducibility and stability for H_2O_2 detection

Fig. 6d illustrates the addition of several most common coexisting electroactive agents such as K^+, NO_3^-, Na^+, Cl^-, UA, and AA within the detection of 0.2 mM H_2O_2 at a set potential of 0.2 V. It can be seen that these compounds do not interfere significantly with the detection process. Reproducibility was also characterized by CV measurements at six individual electrodes in the presence of

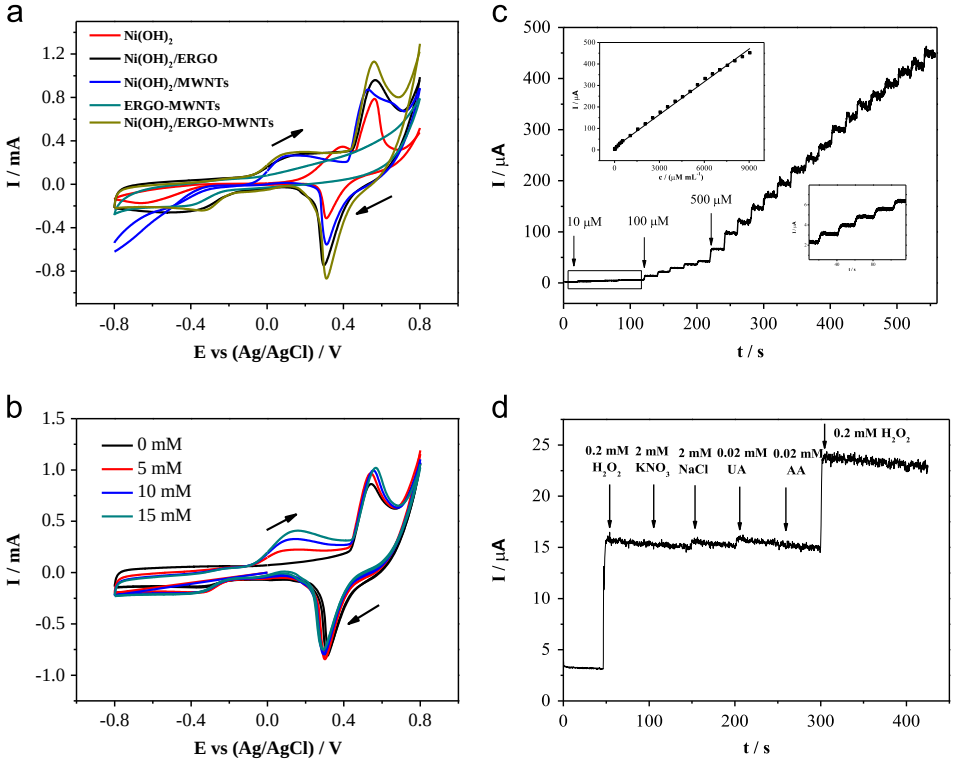

Fig. 6. (a) CVs of $Ni(OH)_2$, ERGO–MWNT, $Ni(OH)_2$/ERGO, $Ni(OH)_2$/MWNT, $Ni(OH)_2$/ERGO–MWNT modified GCE in the presence of 10 mM H_2O_2 at a scan rate of 100 mV s^{-1}. (b) CVs of $Ni(OH)_2$/ ERGO–MWNT/GCE with different concentrations of H_2O_2. The arrows indicate the scan direction. (c) Typical amperometric response of $Ni(OH)_2$/ ERGO–MWNT/GCE to successive addition of H_2O_2, applied potential was 0.2 V. Inset: the corresponding calibration curve of *I-C* obtained by chronoamperometry (upper left) and the amplification of the marked rectangle region (lower right). (d) Interference test at $Ni(OH)_2$/ERGO–MWNT/GCE at 0.2 V. The supporting electrolyte is 0.1 M NaOH.

Table 2
Comparison of the performances of different H_2O_2 sensors.

Sensor	Detection limit (μM)	Linear range (mM)	Sensitivity ($\mu A\ mM^{-1}\ cm^{-2}$)	Reference
Ag–Graphene/GCE	28	0.1–40	Not given	[37]
PtPd/Nafion/CNT	2.5	0.0025–0.125	58.8	[20]
Ag/LDH/GCE	2.2	0.01–19.33	Not given	[21]
CuO/MWNT/GCE	0.16	0.005–0.082	Not given	[38]
Gu_2O/Graphene	20.8	0.3–7.8	Not given	[19]
MnO_2/MWNT	0.0008	0.0012–1.8	1080	[39]
$Ni(OH)_2$/ERGO–MWNT/GCE	4.0	0.01–9.05	717	This work

Table 3
Recovery data for glucose and H_2O_2 determination in real samples using $Ni(OH)_2$/ERGO–MWNT/GCE.

Analyte	Sample type	Spiked (μM)	Found (μM)	RSD[a] (%)	Recovery (%)
Glucose	Urine	100	106.0	3.72	106.0
H_2O_2	Milk	100	104.9	2.39	104.9

[a] Three measurements were taken.

10 mM H_2O_2, and the RSD of the peak currents is estimated to be 2.8%. The sensing stability tests of the prepared electrode were carried out by taking six successive amperometric measurements towards 100 μM H_2O_2. No obvious decline of current response was observed, and an RSD of 6.1% was obtained. These results indicate that the fabrication process of the electrode sensor is reliable and reproducible, and the sensor thus prepared demonstrates a good sensing stability in practical applications.

3.7. Real sample analysis

In order to further verify the reliability of $Ni(OH)_2$/ERGO–MWNT nonenzymatic sensor in practical applications, recoveries of analytes were tested with real samples. For glucose determination, urine obtained from normal human body was used as real sample. For H_2O_2, which is usually used as preservative in food, milk was chosen. The urine and milk samples were diluted 100 times by 0.1 M NaOH before testing. Amperometric measurements were taken when analytes were spiked into the cell. The quantity tested by sensor is compared with actual added amount, as shown in Table 3. It can be seen that the acceptable recoveries of glucose and H_2O_2 indicate the sensor we prepared is sensitive in real samples.

4. Conclusions

An efficient nonenzymatic sensor of GCE modified with a nanocomposite comprising of $Ni(OH)_2$ nanoparticles, ERGO and MWNTs has been fabricated through a convenient, low-cost and green electrochemical method. The water-dispersible GO–MWNT complex exhibits unique features and high charge mobility after electroreduction, performing as an ideal catalytic support for the deposition of $Ni(OH)_2$ nanoparticles. The $Ni(OH)_2$/ERGO–MWNT/GCE displays excellent analytical performance towards glucose and H_2O_2. The synergistic effect of these three components in the nanocomposite endows the sensor with excellent electrochemical performance such as wide linear range, low detection limit, high sensitivity, good selectivity as well as good reproducibility and stability. This kind of ERGO–MWNT complex based nanomaterials has great potential and opens a new way for the development of non-enzymatic biosensors.

Acknowledgments

The authors are grateful for the financial support from the National Natural Science Foundation of China (51125011).

Appendix A. Supplementary material

Supplementary data associated with this article can be found in the online version at http://dx.doi.org/10.1016/j.talanta.2013.12.012.

References

[1] W. Grosse, J. Champavert, S. Gambhir, G.G. Wallace, S.E. Moulton, Carbon 61 (2013) 467–475.
[2] V.K. Gupta, A.K. Jain, S.K. Shoora, Electrochim. Acta 93 (2013) 248–253.
[3] J. Zhao, L.M. Wei, C.H. Peng, Y.J. Su, Z. Yang, L.Y. Zhang, H. Wei, Y.F. Zhang, Biosens. Bioelectron. 47 (2013) 86–91.
[4] H.W. Chang, Y.C. Tsai, C.W. Cheng, C.Y. Lin, P.H. Wu, Sens. Actuat. B: Chem. 183 (2013) 34–39.
[5] Y.Y. Shao, J. Wang, H. Wu, J. Liu, I.A. Aksa, Y.H. Lin, Electroanalysis 22 (2010) 1027–1036.
[6] X.H. Kang, J. Wang, H. Wu, I.A. Aksay, J. Liu, Y.H. Lin, Biosens. Bioelectron. 25 (2009) 901–905.
[7] C.P. Fu, Y.F. Kuang, Z.Y. Huang, X. Wang, N.N. Du, J.H. Chen, H.H. Zhou, Chem. Phys. Lett. 499 (2010) 250–253.
[8] C. Zhang, L.L. Ren, X.Y. Wang, T.X. Liu., J. Phys. Chem. C 114 (2010) 11435–11440.
[9] C.G. Salzmann, S.A. Llewellyn, G. Tobias, M.A.H. Ward, Y. Huh, M.L.H. Green, Adv. Mater. 19 (2007) 883–887.
[10] J. Kim, V.C. Tung, J. Huang, Adv. Energy Mater. 1 (2011) 1052–1057.
[11] W. Lv, F.M. Jin, Q.G. Guo, Q.H. Yang, F.Y. Kang, Electrochim. Acta 73 (2012) 129–135.
[12] J.H. Li, D.Z Kuang, Y.L. Feng, F.X. Zhang, Z.F. Xu, M.Q. Liu, D.P. Wang, Microchim. Acta 180 (2013) 49–58.
[13] D.B. Lu, S.X. Lin, L.T. Wang, C.M. Wang, Talanta 112 (2013) 111–116.
[14] T.Y. Huang, J.H. Huang, H.Y. Wei, K.C. Ho, C.W. Chu, Biosens. Bioelectron. 43 (2013) 173–179.
[15] C. Xia, W. Ning, Electrochem. Commun. 12 (2010) 1581–1584.
[16] J. Luo, S.S. Jiang, H.Y. Zhang, J.Q. Jiang, X.Y. Liu, Anal. Chim. Acta 709 (2012) 47–53.
[17] S.S. Ji, Z Yang, C. Zhang, Y.E. Miao, W.W. Tjiu, J.S. Pan, T.X. Liu, Microchim. Acta 180 (2013) 1127–1134.
[18] J. Chen, W.D. Zhang, J.S. Ye, Electrochem. Commun. 10 (2008) 1268–1271.
[19] M.M. Liu, R. Liu, W. Chen, Biosens. Bioelectron. 45 (2013) 206–212.
[20] K.J. Chen, K.C. Pillai, J. Rick, C. Pan, S. Wang, C. Liu, B. Hwang, Biosens. Bioelectron. 33 (2012) 120–127.
[21] Z. Yang, W.W. Tjiu, W. Fan, T.X. Liu, Electrochim. Acta 90 (2013) 400–407.
[22] W.Z. Li, L. Kuai, Q. Qin, B.Y. Geng, J. Mater. Chem. A 1 (2013) 7111–7117.
[23] Y. Zhang, F.G. Xu, Y.J. Sun, Y. Shi, Z.W. Wen, Z. Li, J. Mater. Chem. 21 (2011) 16949–16954.
[24] A.X. Gu, G.F. Wang, J. Gu, X.J. Zhang, B. Fang, Electrochim. Acta 55 (2010) 7182–7187.
[25] Y.S. Chen, J.H. Huang, Biosens. Bioelectron. 26 (2010) 207–212.
[26] Q. Yan, Z.L. Wang, J. Zhang, Electrochim. Acta 61 (2012) 148–153.
[27] H.L. Guo, X.F. Wang, Q.Y. Qian, F.B. Wang, X.H. Xia, ACS Nano 3 (2009) 2653–2659.
[28] P. Sharma, V. Bhalla, V. Dravid, G. Shekhawat, J.S. Wu, E.S. Prasad, C.R. Suri, Sci. Rep. 2 (2012) 877–893.
[29] L.A. Hutton, M. Vidotti, A.N. Patel, M.E. Newton, P.R. Unwin, J.V. Macpherson, J. Phys. Chem. C 115 (2010) 1649–1658.
[30] J. Lu, J. Yang, J.Z. Wang, A.L. Lim, S. Wang, K.P. Loh, ACS Nano 3 (2009) 2367–2375.
[31] Y. Chang, J. Qiao, Q.L. Liu, L.Z. Shang, Anal. Lett. 41 (2008) 3147–3160.
[32] Y. Liu, H. Teng, H.Q. Hou, T.Y. You, Biosens. Bioelectron. 24 (2009) 3329–3334.
[33] M. Shamsipur, M. Najafi, M.R.M. Hosseini, Bioelectrochemistry 77 (2010) 120–124.
[34] Y.Q. Zhang, Y.Z. Wang, J.B. Jia, J.G. Wang, Sens. Actuat. B: Chem. 171 (2012) 580–587.
[35] K.E. Toghill, L. Xiao, M.A. Phillips, R.G. Compton, Sens. Actuat. B: Chem. 147 (2010) 642–652.
[36] Z.G. Wang, Y. Hu, W.L. Yang, M.J. Zhou, X. Hu, Sensors 12 (2012) 4860–4869.
[37] S. Liu, J.Q. Tian, L. Wang, H.L. Li, Y.W. Zhang, X.P. Sun, Macromolecules 43 (2010) 10078–10083.
[38] K.Y. Zhang, N. Zhang, H. Cai, C. Huang, Microchim. Acta 176 (2012) 137–142.
[39] B. Xun, M.L. Ye, Y.X. Yu, W.D. Zhang, Anal. Chim. Acta 674 (2010) 20–26.